

Félix Laplante Université de Paris Saclay

Christophe Ambroise <sup>1</sup> Laboratoire de Mathématiques et Modélisation d'Evry, Université Paris-Saclay, CNRS, Univ Evry,

Date published: 2025-07-06 Last modified: 2024-07-05

### Abstract

In this paper, Spectral Bridges, a novel clustering algorithm, is introduced. This algorithm builds upon the traditional k-means and spectral clustering frameworks by subdividing data into small Voronoi regions, which are subsequently merged according to a connectivity measure. Drawing inspiration from Support Vector Machine's margin concept, a non-parametric clustering approach is proposed, building an affinity margin between each pair of Voronoi regions. This approach is characterized by minimal hyperparameters and delineation of intricate, non-convex cluster structures.

The numerical experiments underscore Spectral Bridges as a fast, robust, and versatile tool for sophisticated clustering tasks spanning diverse domains. Its efficacy is observed to extend to large-scale scenarios encompassing both real-world and synthetic datasets.

The Spectral Bridge algorithm is implemented both in Python (<https://github.com/flheight/Spectral-Bridges>) and R (<https://github.com/cambroise/spectral-bridges>).

*Keywords:* spectral clustering, vector quantization, scalable, non-parametric

## Contents

1	<b>Contents</b>	
2	<b>1 Introduction</b>	<b>2</b>
3	<b>2 Related Work</b>	<b>3</b>
4	<b>3 Spectral bridges</b>	<b>3</b>
5	3.1 Bridge affinity . . . . .	4
6	3.2 Algorithm . . . . .	5
7	<b>4 Numerical experiments</b>	<b>6</b>
8	4.1 Real-world Data . . . . .	7
9	4.2 Synthetic Data . . . . .	7
10	4.2.1 Datasets Summary & Class Balance . . . . .	7
11	4.3 Metrics . . . . .	7
12	4.4 Platform . . . . .	7
13	4.5 Hyperparameter settings . . . . .	8
14	4.6 Accuracy . . . . .	8
15	4.7 Noise robustness . . . . .	11
16	<b>5 Conclusive remarks</b>	<b>12</b>

---

<sup>1</sup>Corresponding author: [christophe.ambroise@univ-evry.fr](mailto:christophe.ambroise@univ-evry.fr)

17	<b>6 Appendix</b>	<b>12</b>
18	6.1 Derivation of the bridge affinity . . . . .	12
19	6.2 Code . . . . .	13
20	<b>References</b>	<b>14</b>
21	<b>Session information</b>	<b>15</b>

## 22 1 Introduction

23 Clustering is a fundamental technique for exploratory data analysis, organizing a set of objects into  
24 distinct homogeneous groups known as clusters. It is extensively utilized across various fields, such  
25 as biology for gene expression analysis (Eisen et al. 1998), social sciences for community detection in  
26 social networks (Latouche, Birmelé, and Ambroise 2011), and psychology for identifying behavioral  
27 patterns. Clustering is often employed alongside supervised learning as a pre-processing step, helping  
28 to structure and simplify data, thus enhancing the performance and interpretability of subsequent  
29 predictive models (Verhaak et al. 2010). Additionally, clustering can be integrated into supervised  
30 learning algorithms, such as mixture of experts (Jacobs et al. 1991), as part of a multi-objective  
31 strategy.

32 There are numerous approaches to clustering, each defined by how similarity between objects is  
33 measured, either through a similarity measure, a distance metric, or a statistical model.

34 Density-based methods identify regions within the data with a high concentration of points, corre-  
35 sponding to the modes of the joint density. A notable non-parametric example of this approach is  
36 DBSCAN (Ester et al. 1996). In contrast, model-based clustering, such as Gaussian mixture models,  
37 represents a parametric approach to density-based methods. Model-based clustering assumes that  
38 the data is generated from a mixture of underlying probability distributions, typically Gaussian  
39 distributions. Each cluster is viewed as a component of this mixture model, and the Expectation-  
40 Maximization (EM) algorithm is often used to estimate the parameters. This approach provides a  
41 probabilistic framework for clustering, allowing for the incorporation of prior knowledge and the  
42 ability to handle more complex cluster shapes and distributions (McLachlan and Peel 2000).

43 Geometric approaches, such as k-means (MacQueen et al. 1967), are distance-based methods that aim  
44 to partition data by optimizing a criterion reflecting group homogeneity. The k-means++ algorithm  
45 (Arthur and Vassilvitskii 2006) enhances this approach by providing fast, convenient, and interpretable  
46 results. However, a key limitation of these methods is the assumption of linear boundaries between  
47 clusters, implying that clusters are convex. To address non-convex clusters, the kernel trick can be  
48 applied, allowing for a more flexible k-means algorithm. This approach is comparable to spectral  
49 clustering in handling complex cluster boundaries (Dhillon, Guan, and Kulis 2004). The k-means  
50 algorithm can also be interpreted within the framework of model-based clustering under specific  
51 assumptions (Govaert and Nadif 2003), revealing that it is essentially a special case of the more  
52 general Gaussian mixture models, where clusters are assumed to be spherical Gaussian distributions  
53 with equal variance.

54 Graph-based methods represent data as a graph, with vertices symbolizing data points and edges  
55 weighted to indicate the affinity between these points. Spectral clustering can be seen as a relaxed  
56 version of the graph cut algorithm (Shi and Malik 2000). However, traditional spectral clustering faces  
57 significant limitations due to its high time and space complexity, greatly hindering its applicability  
58 to large-scale problems (Von Luxburg 2007).

59 The method we propose aims to find non-convex clusters in large datasets, without relying on a  
60 parametric model, by using spectral clustering based on an affinity that characterizes the local density

of the data. The algorithm described in this paper draws from numerous clustering approaches. The initial intuition is to detect high-density areas. To this end, vector quantization is used to divide the space into a Voronoi tessellation. An original geometric criterion is then employed to detect pairs of Voronoi regions that are either distant from each other or separated by a low-density boundary. Finally, this affinity measure is considered as the weight of an edge in a complete graph connecting the centroids of the tessellation, and a spectral clustering algorithm is used to find a partition of this graph. The only parameters of the algorithm are the number of Voronoi Cells and the number of clusters.

The paper begins with a section dedicated to presenting the context and related algorithms, followed by a detailed description of the proposed algorithm. Experiments and comparisons with reference algorithms are then conducted on both real and synthetic data.

## 2 Related Work

Spectral clustering is a graph-based approach that computes the eigen-vectors of the graph’s Laplacian matrix. This technique transforms the data into a lower-dimensional space, making the clusters more discernible. A standard algorithm like k-means is then applied to these transformed features to identify the clusters (Von Luxburg 2007). Spectral clustering enables capturing complex data structures and discerning clusters based on the connectivity of data points in a transformed space, effectively treating it as a relaxed graph cut problem.

Classical spectral clustering involves two phases: construction of the affinity matrix and eigen-decomposition. Constructing the affinity matrix requires  $O(n^2d)$  time and  $O(n)$  memory, while eigen-decomposition demands  $O(n^3)$  time and  $O(n^2)$  memory, where  $n$  is the data size and  $d$  is the dimension. As  $n$  increases, the computational load escalates significantly (Von Luxburg 2007).

To mitigate this computational burden, one common approach is to sparsify the affinity matrix and use sparse eigen-solvers, reducing memory costs but still requiring computation of all original matrix entries (Von Luxburg 2007). Another strategy is sub-matrix construction. The Nyström method randomly selects  $m$  representatives from the dataset to form an  $n \times m$  affinity sub-matrix (Chen et al. 2010). Cai et al. extended this with the landmark-based spectral clustering method, which uses k-means to determine  $m$  cluster centers as representatives (Cai and Chen 2014). Ultra-scalable spectral clustering (U-SPEC) employs a hybrid representative selection strategy and a fast approximation method for constructing a sparse affinity sub-matrix (Huang et al. 2019).

Other approaches use the properties of the small initial cluster for the affinity computation. Clustering Based on Graph of Intensity Topology (GIT) estimates a global topological graph (topo-graph) between local clusters (Gao et al. 2021). It then uses the Wasserstein Distance between predicted and prior class proportions to automatically cut noisy edges in the topo-graph and merge connected local clusters into final clusters.

The issue of characterizing the affinity between two clusters to create an edge weight is central to the efficiency of a spectral clustering algorithm operating from a submatrix.

Notice that the clustering robustness of many Spectral clustering algorithm heavily relies on the proper selection of kernel parameter, which is difficult to find without prior knowledge (Ng, Jordan, and Weiss 2001).

### 3 Spectral bridges

The proposed algorithm uses k-means centroids for vector quantization defining Voronoi region, and a strategy is proposed to link these regions, with an “affinity” gauged in terms of minimal margin between pairs of classes. These affinities are considered as weight of edges defining a completely connected graph whose vertices are the regions. Spectral clustering on the region provide a partition of the input space. The sole parameters of the algorithm are the number of Voronoi region and the number of final cluster.

#### 3.1 Bridge affinity

The basic idea involves calculating the difference in inertia achieved by projecting onto a segment connecting two centroids, rather than using the two centroids separately (See Figure Figure 1). If the difference is small, it suggests a low density between the classes. Conversely, if this difference is large, it indicates that the two classes may reside within the same densely populated region.

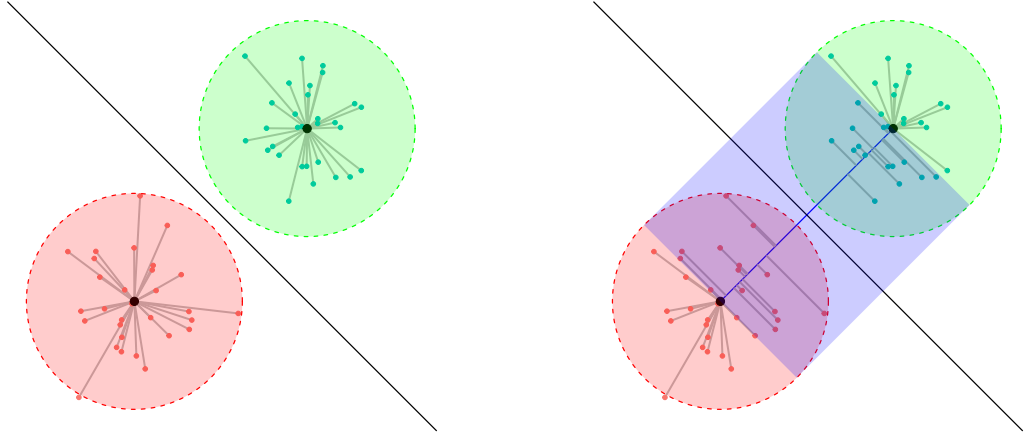


Figure 1: Balls (left) versus Bridge (right). The inertia of each structure is the sum of the squared distances represented by grey lines.

Let us consider a sample  $X = (\mathbf{x}_i)_{i \in \{1, \dots, n\}}$  of vectors  $\mathbf{x}_i \in \mathbb{R}^p$  and a set of  $m$  coding vectors  $(\boldsymbol{\mu}_k)_{k \in \{1, \dots, m\}}$  defining a partition  $P = \{\mathcal{V}_1, \dots, \mathcal{V}_m\}$  of  $\mathbb{R}^p$  into  $m$  Voronoi regions:

$$\mathcal{V}_k = \{\mathbf{x} \in \mathbb{R}^n \mid \|\mathbf{x} - \boldsymbol{\mu}_k\| \leq \|\mathbf{x} - \boldsymbol{\mu}_j\| \text{ for all } j \neq k\}.$$

In the following a ball denotes the subset of  $X$  in a Voronoi region. The inertia of two balls  $\mathcal{V}_k$  and  $\mathcal{V}_l$  is

$$I_{kl} = \sum_{\mathbf{x}_i \in \mathcal{V}_k} \|\mathbf{x}_i - \boldsymbol{\mu}_k\|^2 + \sum_{\mathbf{x}_i \in \mathcal{V}_l} \|\mathbf{x}_i - \boldsymbol{\mu}_l\|^2.$$

We define a bridge as a structure defined by a segment connecting two centroids  $\boldsymbol{\mu}_k$  and  $\boldsymbol{\mu}_l$ . The inertia of a bridge between  $\mathcal{V}_k$  and  $\mathcal{V}_l$  is defined as

$$B_{kl} = \sum_{\mathbf{x}_i \in \mathcal{V}_k \cup \mathcal{V}_l} \|\mathbf{x}_i - \mathbf{p}_{kl}(\mathbf{x}_i)\|^2,$$

where

$$\mathbf{p}_{kl}(\mathbf{x}_i) = \boldsymbol{\mu}_k + t_i(\boldsymbol{\mu}_l - \boldsymbol{\mu}_k),$$

120 with

$$t_i = \min \left( 1, \max \left( 0, \frac{\langle \mathbf{x}_i - \boldsymbol{\mu}_k | \boldsymbol{\mu}_l - \boldsymbol{\mu}_k \rangle}{\|\boldsymbol{\mu}_l - \boldsymbol{\mu}_k\|^2} \right) \right).$$

121 Considering two centroids, the normalized average of the difference between Bridge and balls  
122 inertia (See [Appendix](#)) constitutes the basis of our affinity measure between to regions:

$$\begin{aligned} \frac{B_{kl} - I_{kl}}{(n_k + n_l)\|\boldsymbol{\mu}_k - \boldsymbol{\mu}_l\|^2} &= \frac{\sum_{\mathbf{x}_i \in \mathcal{V}_k} \langle \mathbf{x}_i - \boldsymbol{\mu}_k | \boldsymbol{\mu}_l - \boldsymbol{\mu}_k \rangle^2 + \sum_{\mathbf{x}_i \in \mathcal{V}_l} \langle \mathbf{x}_i - \boldsymbol{\mu}_l | \boldsymbol{\mu}_k - \boldsymbol{\mu}_l \rangle^2}{(n_k + n_l)\|\boldsymbol{\mu}_k - \boldsymbol{\mu}_l\|^4}, \\ &= \frac{\sum_{\mathbf{x}_i \in \mathcal{V}_k \cup \mathcal{V}_l} \alpha_i^2}{n_k + n_l}, \end{aligned}$$

123 where

$$\alpha_i = \begin{cases} t_i, & \text{if } t_i \in [0, 1/2], \\ 1 - t_i, & \text{if } t_i \in ]1/2, 1]. \end{cases}$$

124 The basic intuition behind this affinity is that  $t_i$  represents the relative position of the projection of  $\mathbf{x}_i$   
125 on the segment  $[\boldsymbol{\mu}_k, \boldsymbol{\mu}_l]$ .  $\alpha_i$  represents the relative position on the segment, with the centroid of the  
126 class to which  $\mathbf{x}_i$  belongs as the starting point.

127 The boundary that separates the two clusters defined by centroids  $\boldsymbol{\mu}_k$  and  $\boldsymbol{\mu}_l$  is a hyperplane. This  
128 hyperplane is orthogonal to the line segment connecting the centroids and intersects this segment at  
129 its midpoint.

130 If we consider all points  $\mathbf{x}_i \in \mathcal{V}_k \cup \mathcal{V}_l$  which are not projected on centroids but somewhere on the  
131 segment, the distance from a point to the hyperplane is

$$\|\mathbf{p}_{kl}(\mathbf{x}_i) - \boldsymbol{\mu}_{kl}\| = (1/2 - \alpha_i)\|\boldsymbol{\mu}_k - \boldsymbol{\mu}_l\|.$$

132 This distance is similar to the concept of margin in Support Vector Machine (Cortes and Vapnik 1995).  
133 When the  $\alpha_i$  values are small (close to zero since  $\alpha_i \in [0, 1/2]$ ), the margins to the hyperplane are  
134 large, indicating a low density between the classes. Conversely, if the margins are small, it suggests  
135 that the two classes may reside within the same densely populated region. Consequently, the sum of  
136 the  $\alpha_i$  or  $\alpha_i^2$  increases with the density of the region between the classes.

137 Note that the criterion is local and indicates the relative difference in densities between the balls and  
138 the bridge, rather than evaluating a global score for the densities of the structures.

139 Eventually, we define the bridge affinity between centroids  $k$  and  $l$  as:

$$a_{kl} = \begin{cases} 0, & \text{if } k = l, \\ \frac{\sum_{\mathbf{x}_i \in \mathcal{V}_k \cup \mathcal{V}_l} \alpha_i^2}{n_k + n_l}, & \text{otherwise.} \end{cases}$$

140 To allow points with large margin to dominate and make the algorithm more robust to noise and  
141 outliers we consider the following exponential transformation:

$$\tilde{a}_{kl} = g(a_{kl}) = \exp \sqrt{(a_{kl})}.$$

## 3.2 Algorithm

The Spectral Bridges algorithm first identifies local clusters to define Voronoi regions, computes edges with affinity weights between these regions, and ultimately cuts edges between regions with low inter-region density to determine the final clusters (See Algorithm Algorithm 1 and Figure Figure 2).

In spectral clustering, the time complexity is usually dominated by the eigendecomposition step, which is  $O(n^3)$ . However, in the case of Spectral Bridges, the kmeans algorithm has a time complexity of  $O(n \times m \times p)$ . For datasets with large  $n$ , this can be more significant than the  $O(m^3)$  time complexity of the Spectral Bridges eigendecomposition.

---

### Algorithm 1 Spectral Bridges

---

```

1: procedure SPECTRALBRIDGES( $X, k, m$ )  $\triangleright$   $X$ : input dataset,  $k$ : number of clusters,  $m$ : number of
   Voronoi regions
2:   Step 1: Vector Quantization
3:    $centroids, voronoiRegions \leftarrow \text{KMEANS}(X, m)$   $\triangleright$  Initial centroids and Voronoi Regions using
   k-means++
4:   Step 2: Affinity Computation
5:    $A = \{g(a_{kl})\}_{kl} \leftarrow \text{AFFINITY}(X, centroids, voronoiRegions)$ 
6:   Step 3: Spectral Clustering  $\triangleright$  Affect each region to a cluster
7:    $labels \leftarrow \text{SPECTRALCLUSTERING}(A, k)$ 
8:   Step 4: Propagate  $\triangleright$  Affect each data point to the cluster of its region
9:    $clusters \leftarrow \text{PROPAGATE}(X, labels, voronoiRegions)$ 
10:  return  $clusters$   $\triangleright$  Cluster labels for data points in  $X$ 
11: end procedure

```

---

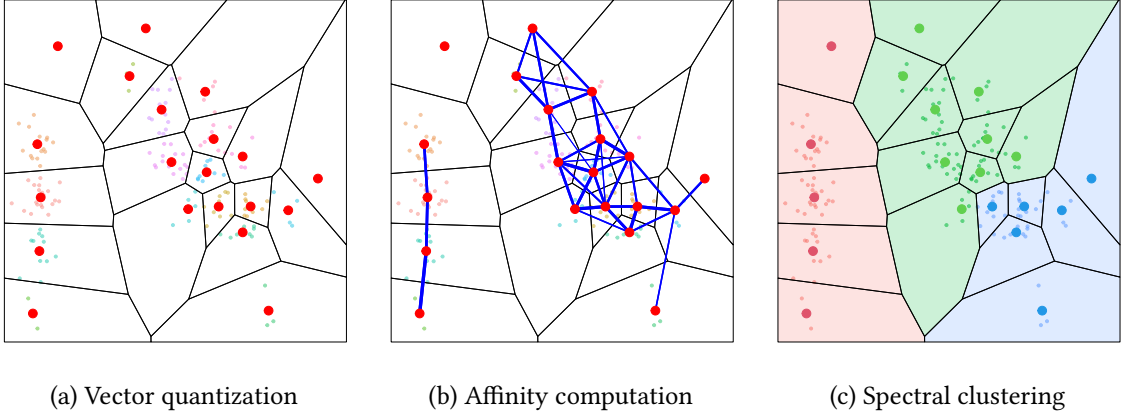


Figure 2: Illustration of the Spectral bridges algorithm with the Iris dataset (first principal plane). Vector quantization (Step 1 of Algorithm Algorithm 1), Affinity computation (Step 2 of Algorithm Algorithm 1), Spectral clustering and spreading (Step 3-4 of Algorithm Algorithm 1).

## 4 Numerical experiments

In this section, we present the results obtained from testing our algorithm on various datasets, both small and large scale, including real-world and well-known synthetic datasets. These experiments assess the accuracy, time and space complexity, ease of use, robustness, and adaptability of our algorithm. We compare **Spectral Bridges (SB)** against several state-of-the-art methods, including **k-means++ (KM)** (MacQueen et al. 1967; Arthur and Vassilvitskii 2006), **Expectation-Maximization**

(**EM**) (Dempster, Laird, and Rubin 1977), **Ward Clustering (WC)** (Ward Jr 1963), and **DBSCAN (DB)** (Ester et al. 1996). This comparison establishes baselines across centroid-based clustering algorithms, hierarchical methods, and density-based methods.

The algorithms are evaluated on both raw and PCA-processed data with varying dimensionality. For synthetic datasets, Gaussian and/or uniform noise is introduced to assess the robustness of the algorithm.

## 4.1 Real-world Data

- **MNIST**: A large dataset containing 60,000 handwritten digit images in ten balanced classes, commonly used for image processing benchmarks. Each image consists of  $28 \times 28 = 784$  pixels.
- **UCI ML Breast Cancer Wisconsin**: A dataset featuring computed attributes from digitized images of fine needle aspirates (FNA) of breast masses, used to predict whether a tumor is malignant or benign.

## 4.2 Synthetic Data

- **Impossible**: A synthetic dataset designed to challenge clustering algorithms with complex patterns.
- **Moons**: A two-dimensional dataset with two interleaving half circles.
- **Circles**: A synthetic dataset of points arranged in two non-linearly separable circles.
- **Smile**: A synthetic dataset with points arranged in the shape of a smiling face, used to test the separation of non-linearly separable data.

### 4.2.1 Datasets Summary & Class Balance

Table 1: Datasets Summary & Class Balance

Dataset	#Dims	#Samples	#Classes	Class Proportions
MNIST	784	60000	10	9.9%, 11.2%, 9.9%, 10.3%, 9.7%, 9%, 9.9%, 10.4%, 9.7%, 9.9%
Breast Cancer	30	569	2	37.3%, 62.7%
Impossible	2	3594	7	24.8%, 18.8%, 11.3%, 7.5%, 12.5%, 12.5%, 12.5%
Moons	2	1000	2	50%, 50%
Circles	2	1000	2	50%, 50%
Smile	2	1000	4	25%, 25%, 25%, 25%

Class proportions are presented in ascending order starting from label 0.

## 4.3 Metrics

To evaluate the performance of the clustering algorithm, the Adjusted Rand Index (**ARI**) (Halkidi, Batistakis, and Vazirgiannis 2002) and Normalized Mutual Information (**NMI**) (Cover and Thomas 1991) are used. ARI measures the similarity between two clustering results, ranging from  $-0.5$  to  $1$ , with  $1$  indicating perfect agreement. NMI ranges from  $0$  to  $1$ , with higher values indicating better clustering quality. In some tests, the variability of scores across multiple runs is also reported due to the random initialization in k-means, though k-means++ generally provides stable and reproducible results.

## 4.4 Platform

All experiments were conducted on an Archlinux machine with Linux 6.9.3 Kernel, 8GB of RAM, and an AMD Ryzen 3 7320U processor.

## 4.5 Hyperparameter settings

We set the hyperparameters of our algorithm based on the size of each dataset,  $n$ , and the number of clusters,  $K$ . A larger number of clusters typically suggests that a higher value for the number of Voronoi regions is optimal. Conversely, using a high number of Voronoi regions for a small dataset might result in nearly empty regions that do not adequately represent any local structure.

A good yet not very precise way of setting the number of Voronoi regions  $m$  is to observe the Within Cluster Sum of Squares (WCSS) or inertia in a way akin to the elbow method. Since  $m$  should be set to a value strictly greater than  $K$ , we plot the WCSS for varying values of  $m$ , and find a value such that the WCSS- $m$  relationship becomes quasi-linear.

By adjusting  $m$  in this manner, we aim to balance the need for detailed representation with the risk of overfitting, ensuring that each Voronoi region meaningfully captures the underlying data distribution.

For other algorithms, such as DBSCAN, labels were used to determine the best hyperparameter values to compare our method against the “best case scenario”, thus putting the Spectral Bridges algorithm at a voluntary disadvantage.

## 4.6 Accuracy

We first evaluated our algorithm’s accuracy on the MNIST dataset. Metrics were collected to compare our method with k-means++, EM, and Ward clustering. Metric were estimated by taking the empirical average over 10 consecutive runs with the same random seed for each method. Since our computational capabilities were too limited, we sampled 20000 (one third) data points at random. This sample is not fixed and changes for each iteration.

Let  $h$  denote the embedding dimension of the dataset. We tested our method on the raw MNIST dataset without preprocessing ( $h = 784$ ) and after reducing its dimension using PCA to  $h \in \{8, 16, 32, 64\}$  (see Figure 3).

For visualization purposes, we projected with UMAP the predicted clusters from our algorithm and other methods to compare them against the ground truth labels to better understand the cluster shapes (see table 2). Note that the projection was not used in our experiments as an embedding, and thus does not play any role in the clustering process itself. As a matter of fact, the embedding used was obtained with PCA,  $h = 32$  and 250 Voronoi regions. Note that the label colors match the legend only in the case of the ground truth data. Indeed, the ordering of the labels have no impact on clustering quality.

We also put our algorithm to the test against the same competitors using scikit-learn’s UCI Breast Cancer data. Once again, our method performs well although the advantage is not as obvious in this case (see Figure 5). However, in none of our tests has it ranked worse than k-means++. The results are displayed as a boxplot generated from 200 iterations of each algorithm using a different seed, in order to better grasp the variability lying in the seed dependent nature of the k-means++, Expectation Maximization and Spectral Bridges algorithms.

Since the Spectral Bridges algorithm is expected to excel at discerning complex and intricate cluster structures, an array of four toy datasets was collected, as illustrated in Figure Figure 6.



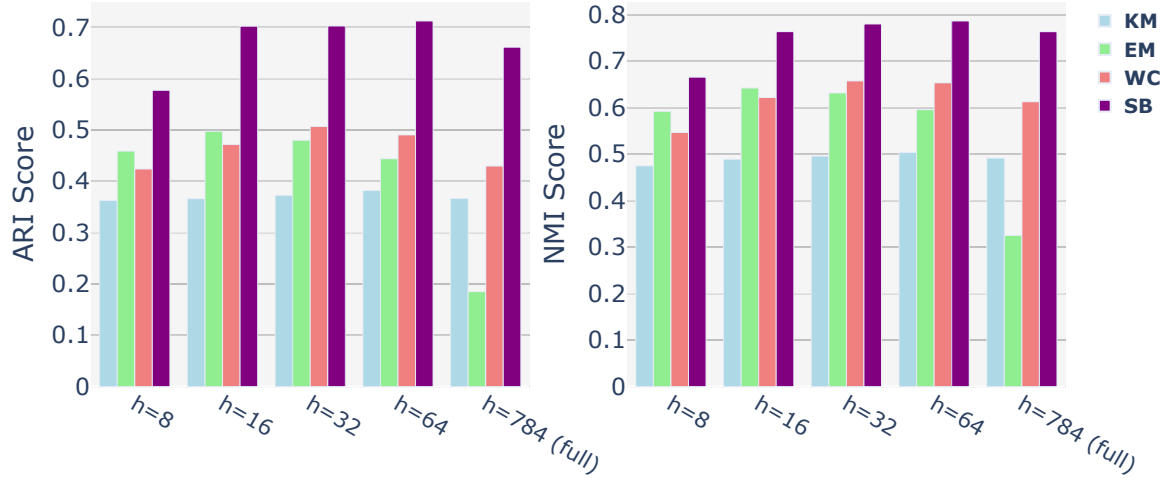


Figure 3: ARI and NMI scores of **k-means++** (blue), **EM** (green), **Ward Clustering** (red), and **Spectral Bridges** (purple) on PCA embedding and full MNIST.

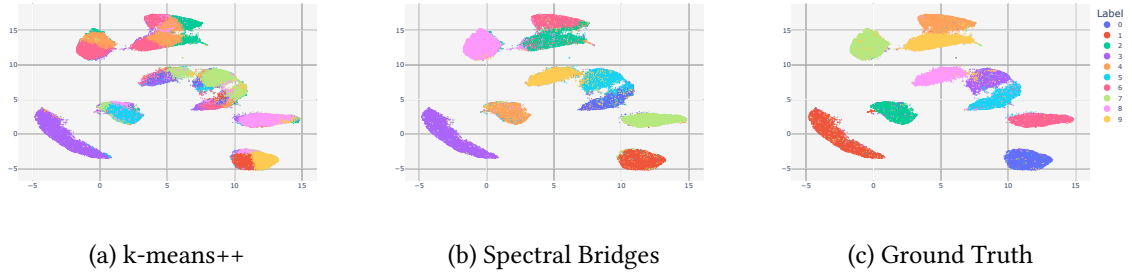


Figure 4: UMAP projection of predicted clusters against the ground truth labels.

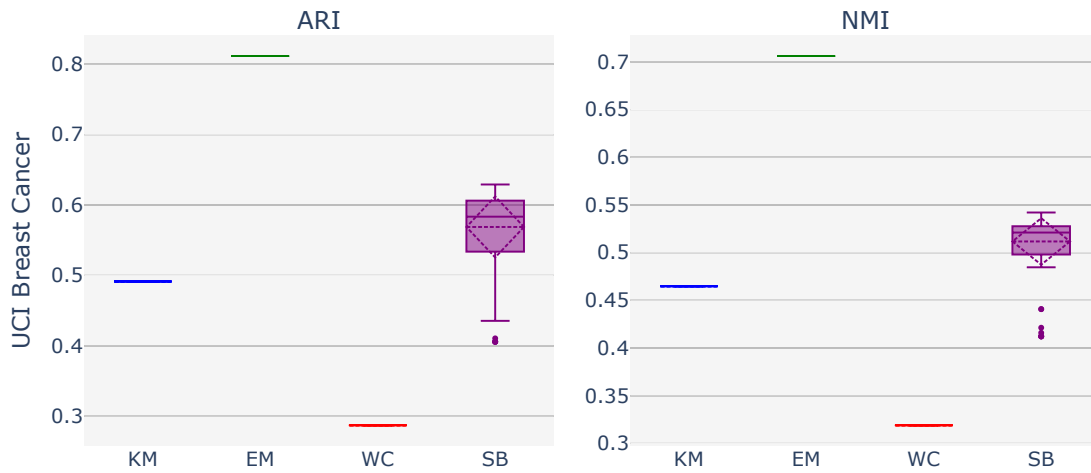


Figure 5: ARI and NMI scores of **k-means++** (blue), **EM** (green), **Ward Clustering** (red), and **Spectral Bridges** (purple) on the UCI Breast Cancer dataset.

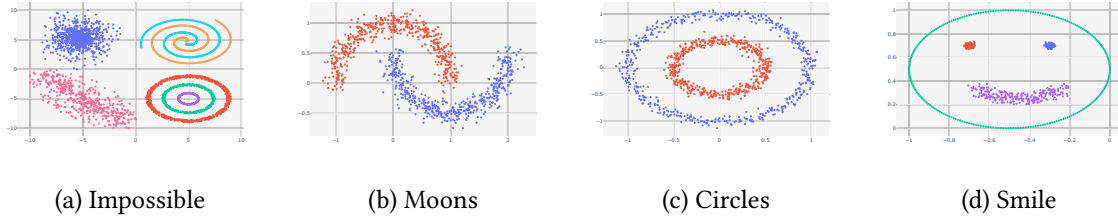


Figure 6: Four toy datasets.

227 Multiple algorithms, including the proposed one, were benchmarked in the exact same manner  
 228 as for the UCI Breast Cancer data. The results show that the proposed method outperforms all  
 229 tested algorithms (DBSCAN, k-means++, Expectation Maximization, and Ward Clustering) while  
 230 requiring few hyperparameters. As previously discussed, DBSCAN’s parameters were optimized  
 231 using the ground truth labels to represent a best-case scenario; however, in practical applications,  
 232 suboptimal performance is more likely. Despite this optimization, the Spectral-Bridge algorithm still  
 233 demonstrates superior ability to capture and represent the underlying cluster structures.

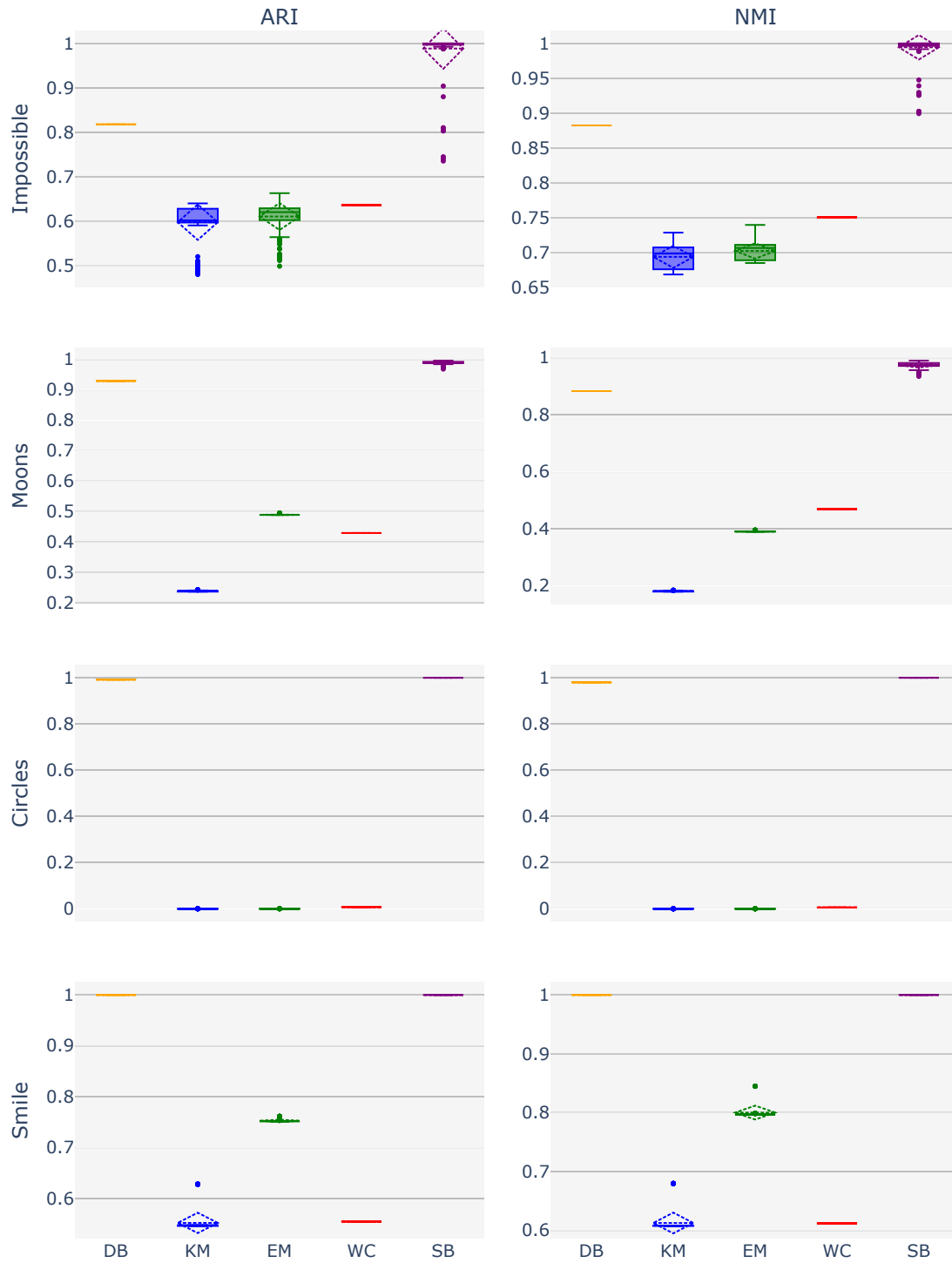


Figure 7: ARI and NMI scores of Spectral Bridges and competitors on standard synthetic toy datasets

## 4.7 Noise robustness

To evaluate the noise robustness of the algorithm, two experimental setups were devised: one involved introducing Gaussian-distributed perturbations to the data, and the other involved concatenating

uniformly distributed points within a predefined rectangular region (determined by the span of the dataset) to the existing dataset. As illustrated in Figure Figure 8, the tests demonstrate that in both scenarios, the algorithm exhibits a high degree of insensitivity to noise.

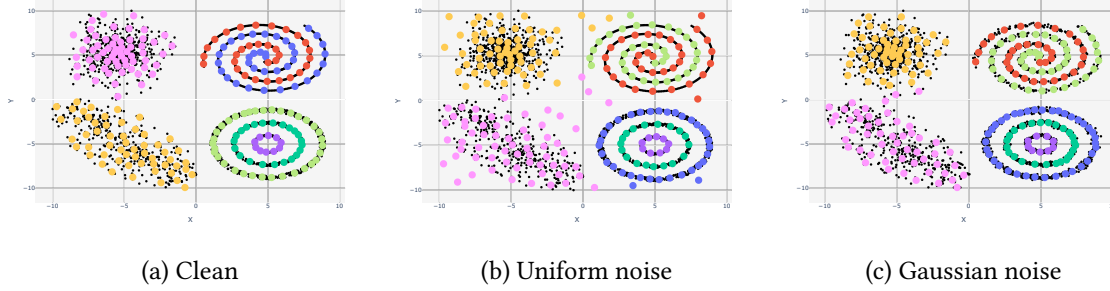


Figure 8: Three representations of the algorithm’s predicted cluster centers are displayed as colored dots, with each point of the Impossible dataset shown as a small black dot. In the left graph, the dataset is unmodified. In the center graph, 250 uniformly distributed samples were added. In the right graph, Gaussian noise perturbations with  $\sigma = 0.1$  were applied.

## 5 Conclusive remarks

Spectral Bridges is an original clustering algorithm which presents a novel approach by integrating the strengths of traditional kmeans and spectral clustering frameworks. This algorithm utilizes a simple affinity measure for spectral clustering, which is derived from the minimal margin between pairs of Voronoi regions.

The algorithm demonstrates impressive scalability, handling large datasets efficiently through a balanced computational complexity between the k-means clustering and eigendecomposition steps. As a non-parametric method, Spectral Bridges does not rely on strong assumptions about data distribution, enhancing its versatility across various data types. It performs exceptionally well with both synthetic and real-world data and consistently outperforms conventional clustering algorithms such as k-means, DBSCAN, and mixture models.

The design of Spectral Bridges ensures robustness to noise, a significant advantage in real-world applications. Additionally, the algorithm requires minimal hyperparameters, primarily the number of Voronoi regions, making it straightforward to tune and deploy.

Furthermore, Spectral Bridges can be kernelized, allowing it to handle data in similarity space directly, which enhances its flexibility and applicability. Overall, Spectral Bridges is a powerful, robust, and scalable clustering algorithm that offers significant improvements over traditional methods, making it an excellent tool for advanced clustering tasks across numerous domains.

## 6 Appendix

### 6.1 Derivation of the bridge affinity

We denote a bridge as a segment connecting two centroids  $\mu_k$  and  $\mu_l$ . The inertia of a bridge between  $\mathcal{V}_k$  and  $\mathcal{V}_l$  is defined as

$$B_{kl} = \sum_{\mathbf{x}_i \in \mathcal{V}_k \cup \mathcal{V}_l} \|\mathbf{x}_i - \mathbf{p}_{kl}(\mathbf{x}_i)\|^2,$$

262 where

$$\mathbf{p}_{kl}(\mathbf{x}_i) = \boldsymbol{\mu}_k + t_i(\boldsymbol{\mu}_l - \boldsymbol{\mu}_k),$$

263 with

$$t_i = \min \left( 1, \max \left( 0, \frac{\langle \mathbf{x}_i - \boldsymbol{\mu}_k | \boldsymbol{\mu}_l - \boldsymbol{\mu}_k \rangle}{\|\boldsymbol{\mu}_l - \boldsymbol{\mu}_k\|^2} \right) \right).$$

264  $B_{kl}$ , the bridge inertia between centroids  $k$  and  $l$ , can be expressed as the sum of three terms, which  
265 represents the projection onto each centroids and onto the segment:

$$B_{kl} = \sum_{i|t_i=0} \|\mathbf{x}_i - \boldsymbol{\mu}_k\|^2 + \sum_{i|t_i=1} \|\mathbf{x}_i - \boldsymbol{\mu}_l\|^2 + \sum_{i|t_i \in ]0,1[} \|\mathbf{x}_i - \mathbf{p}_{kl}(\mathbf{x}_i)\|^2.$$

266 The last term may be decomposed in two parts corresponding to the points of the two Voronoi  
267 regions which are projected on the segment:

$$\sum_{i|t_i \in ]0,1[} \|\mathbf{x}_i - \mathbf{p}_{kl}(\mathbf{x}_i)\|^2 = \sum_{i|t_i \in ]0, \frac{1}{2}[} \|\mathbf{x}_i - \mathbf{p}_{kl}(\mathbf{x}_i)\|^2 + \sum_{i|t_i \in [\frac{1}{2}, 1[} \|\mathbf{x}_i - \mathbf{p}_{kl}(\mathbf{x}_i)\|^2$$

268 and each part further decomposed using Pythagore

$$\begin{aligned} \sum_{i|t_i \in ]0, \frac{1}{2}[} \|\mathbf{x}_i - \mathbf{p}_{kl}(\mathbf{x}_i)\|^2 &= \sum_{i|t_i \in ]0, \frac{1}{2}[} \|\mathbf{x}_i - \boldsymbol{\mu}_k\|^2 - \sum_{i|t_i \in ]0, \frac{1}{2}[} \|\boldsymbol{\mu}_k - \mathbf{p}_{kl}(\mathbf{x}_i)\|^2 \\ &= \sum_{i|t_i \in ]0, \frac{1}{2}[} \|\mathbf{x}_i - \boldsymbol{\mu}_k\|^2 - \sum_{i|t_i \in ]0, \frac{1}{2}[} t_i(\boldsymbol{\mu}_k - \boldsymbol{\mu}_l)^2, \end{aligned}$$

$$\begin{aligned} \sum_{i|t_i \in [\frac{1}{2}, 1[} \|\mathbf{x}_i - \mathbf{p}_{kl}(\mathbf{x}_i)\|^2 &= \sum_{i|t_i \in ]0, \frac{1}{2}[} \|\mathbf{x}_i - \boldsymbol{\mu}_l\|^2 - \sum_{i|t_i \in ]0, \frac{1}{2}[} \|\boldsymbol{\mu}_l - \mathbf{p}_{kl}(\mathbf{x}_i)\|^2 \\ &= \sum_{i|t_i \in [\frac{1}{2}, 1[} \|\mathbf{x}_i - \boldsymbol{\mu}_k\|^2 - \sum_{i|t_i \in ]0, \frac{1}{2}[} \|(1 - t_i)(\boldsymbol{\mu}_k - \boldsymbol{\mu}_l)\|^2 \end{aligned}$$

269 Thus

$$\begin{aligned} B_{kl} - I_{kl} &= \sum_{i|t_i \in ]0, \frac{1}{2}[} t_i^2 \|\boldsymbol{\mu}_k - \boldsymbol{\mu}_l\|^2 + \sum_{i|t_i \in [\frac{1}{2}, 1[} (1 - t_i)^2 \|\boldsymbol{\mu}_k - \boldsymbol{\mu}_l\|^2, \\ \frac{B_{kl} - I_{kl}}{\|\boldsymbol{\mu}_k - \boldsymbol{\mu}_l\|^2} &= \sum_{i|t_i \in ]0, \frac{1}{2}[} t_i^2 + \sum_{i|t_i \in [\frac{1}{2}, 1[} (1 - t_i)^2, \\ \frac{B_{kl} - I_{kl}}{(n_k + n_l) \|\boldsymbol{\mu}_k - \boldsymbol{\mu}_l\|^2} &= \frac{\sum_{\mathbf{x}_i \in \mathcal{V}_k} \langle \mathbf{x}_i - \boldsymbol{\mu}_k | \boldsymbol{\mu}_l - \boldsymbol{\mu}_k \rangle_+^2 + \sum_{\mathbf{x}_i \in \mathcal{V}_l} \langle \mathbf{x}_i - \boldsymbol{\mu}_l | \boldsymbol{\mu}_k - \boldsymbol{\mu}_l \rangle_+^2}{(n_k + n_l) \|\boldsymbol{\mu}_k - \boldsymbol{\mu}_l\|^4}. \end{aligned}$$

## 270 6.2 Code

271 Numerical experiments have been conducted in Python. The python scripts to reproduce the  
272 simulations and figures are available at <https://github.com/flheight/Spectral-Bridges>. A R package  
273 implementing the algorithm is also available (<https://github.com/cambroise/spectral-bridges>).

## References

- Arthur, David, and Sergei Vassilvitskii. 2006. "K-Means++: The Advantages of Careful Seeding." Technical Report 2006-13. Stanford InfoLab; Stanford. <http://ilpubs.stanford.edu:8090/778/>.
- Cai, Deng, and Xinlei Chen. 2014. "Large Scale Spectral Clustering via Landmark-Based Sparse Representation." *IEEE Transactions on Cybernetics* 45 (8): 1669–80.
- Chen, Wen-Yen, Yangqiu Song, Hongjie Bai, Chih-Jen Lin, and Edward Y Chang. 2010. "Parallel Spectral Clustering in Distributed Systems." *IEEE Transactions on Pattern Analysis and Machine Intelligence* 33 (3): 568–86.
- Cortes, Corinna, and Vladimir Vapnik. 1995. "Support-Vector Networks." *Machine Learning* 20 (3): 273–97.
- Cover, Thomas M, and Joy A Thomas. 1991. "Information Theory and the Stock Market." *Elements of Information Theory*. Wiley Inc., New York, 543–56.
- Dempster, Arthur P, Nan M Laird, and Donald B Rubin. 1977. "Maximum Likelihood from Incomplete Data via the EM Algorithm." *Journal of the Royal Statistical Society: Series B (Methodological)* 39 (1): 1–22.
- Dhillon, Inderjit S, Yuqiang Guan, and Brian Kulis. 2004. "Kernel k-Means, Spectral Clustering and Normalized Cuts." In *Proceedings of the Tenth ACM SIGKDD International Conference on Knowledge Discovery and Data Mining*, 551–56. ACM.
- Eisen, Michael B., Paul T. Spellman, Patrick O. Brown, and David Botstein. 1998. "Cluster Analysis and Display of Genome-Wide Expression Patterns." *Proceedings of the National Academy of Sciences* 95 (25): 14863–68.
- Ester, Martin, Hans-Peter Kriegel, Jörg Sander, Xiaowei Xu, et al. 1996. "A Density-Based Algorithm for Discovering Clusters in Large Spatial Databases with Noise." In *Kdd*, 96:226–31.
- Gao, Zhangyang, Haitao Lin, Cheng Tan, Lirong Wu, Stan Li, et al. 2021. "Git: Clustering Based on Graph of Intensity Topology." *arXiv Preprint arXiv:2110.01274*.
- Govaert, Gérard, and Mohamed Nadif. 2003. "Clustering with Block Mixture Models." *Pattern Recognition* 36 (2): 463–73.
- Halkidi, Maria, Yannis Batistakis, and Michalis Vazirgiannis. 2002. "Cluster Validity Methods: Part i." *ACM SIGMOD Record* 31 (2): 40–45.
- Huang, Dong, Chang-Dong Wang, Jian-Sheng Wu, Jian-Huang Lai, and Chee-Keong Kwoh. 2019. "Ultra-Scalable Spectral Clustering and Ensemble Clustering." *IEEE Transactions on Knowledge and Data Engineering* 32 (6): 1212–26.
- Jacobs, Robert A, Michael I Jordan, Steven J Nowlan, and Geoffrey E Hinton. 1991. "Adaptive Mixtures of Local Experts." *Neural Computation* 3 (1): 79–87.
- Latouche, Pierre, Etienne Birmelé, and Christophe Ambroise. 2011. "Overlapping stochastic block models with application to the French political blogosphere." *The Annals of Applied Statistics* 5 (1): 309–36. <https://doi.org/10.1214/10-AOAS382>.
- MacQueen, James et al. 1967. "Some Methods for Classification and Analysis of Multivariate Observations." In *Proceedings of the Fifth Berkeley Symposium on Mathematical Statistics and Probability*, 1:281–97. Oakland, CA, USA.
- McLachlan, Geoffrey J., and David Peel. 2000. *Finite Mixture Models*. New York: Wiley-Interscience.
- Ng, Andrew, Michael Jordan, and Yair Weiss. 2001. "On Spectral Clustering: Analysis and an Algorithm." *Advances in Neural Information Processing Systems* 14.
- Shi, Jianbo, and Jitendra Malik. 2000. "Normalized Cuts and Image Segmentation." *IEEE Transactions on Pattern Analysis and Machine Intelligence* 22 (8): 888–905.
- Verhaak, Roel G. W., Katherine A. Hoadley, Elizabeth Purdom, Victoria Wang, Yuexin Qi, Matthew D. Wilkerson, Charlie R. Miller, et al. 2010. "Integrated Genomic Analysis Identifies Clinically Relevant Subtypes of Glioblastoma Characterized by Abnormalities in PDGFRA, IDH1, EGFR, and NF1." *Cancer Cell* 17 (1): 98–110.

323 Von Luxburg, Ulrike. 2007. "A Tutorial on Spectral Clustering." *Statistics and Computing* 17: 395–416.  
324 Ward Jr, Joe H. 1963. "Hierarchical Grouping to Optimize an Objective Function." *Journal of the*  
325 *American Statistical Association* 58 (301): 236–44.

## 326 Session information

327 R version 4.4.1 (2024-06-14 ucrt)  
328 Platform: x86\_64-w64-mingw32/x64  
329 Running under: Windows 11 x64 (build 22631)  
330  
331 Matrix products: default  
332  
333 locale:  
334 [1] LC\_COLLATE=French\_France.utf8 LC\_CTYPE=French\_France.utf8  
335 [3] LC\_MONETARY=French\_France.utf8 LC\_NUMERIC=C  
336 [5] LC\_TIME=French\_France.utf8  
337  
338  
339 time zone: Europe/Paris  
340 tzcode source: internal  
341  
342 attached base packages:  
343 [1] stats graphics grDevices utils datasets methods base  
344  
345 loaded via a namespace (and not attached):  
346 [1] compiler\_4.4.1 fastmap\_1.2.0 cli\_3.6.3 tools\_4.4.1  
347 [5] htmltools\_0.5.8.1 yaml\_2.3.8 rmarkdown\_2.27 knitr\_1.47  
348 [9] jsonlite\_1.8.8 xfun\_0.45 digest\_0.6.36 rlang\_1.1.4  
349 [13] evaluate\_0.24.0